Automatic brain tumor segmentation and tumor tissue classification based on multiple MR protocols

A. Franz[1], H. Tschampa[2], A. Müller[2], S. Remmele[1], J. Keupp[1], J. Gieseke[3], H. H. Schild[2], and P. Mürtz[2]
[1]Philips Research, Hamburg, Germany, [2]Department of Radiology, University Hospital Bonn, Bonn, Germany, [3]Philips Healthcare, Hamburg, Germany

Introduction

Segmentation of brain tumors in Magnetic Resonance (MR) images and classification of the tumor tissue into vital, necrotic, and perifocal edematous is required in a variety of clinical applications, as tumor diagnosis, grading and follow-up studies via volumetry [1,2], radiation therapy planning [3], surgery planning [4], or automatic region-of-interest segmentation for quantitative analysis, as vascularity-related parameters [5]. Manual delineation of the tumor tissue boundaries is a tedious and error-prone task, and the results are not reproducible. Hence, an automatic procedure for segmenting and classifying brain tumor tissue is needed. A variety of segmentation approaches for brain tumors in MR images can be found in the literature, which are mainly based on statistical [6-8] and variational [9-12] methods. Tumor tissue classification mostly requires information of several MR protocols and contrasts, as T1, T1contrast enhanced (T1CE), T2, FLAIR, MPRAGE, VASO [4,13-16]. The aim of this work was to realize a segmentation tool based on a 3D region growing algorithm for depiction of vital tumor, necrotic area and perifocal edema in T1CE and FLAIR images. Both image types are included in brain tumor protocols that are used in regular clinical routine.

Methods

A 3D region growing algorithm [17] was alternately applied on the T1CE and FLAIR images. The starting point was manually set. The image intensity at the starting point was used as initial upper threshold of the search range in both contrasts. As soon as an image voxel with a higher intensity was found, the upper threshold was updated, and the region growing started again at the location of this newly found maximum intensity. This resulted in a robust segmentation which was independent of the location of the starting point within the tumor. The lower threshold of the search range was related to the upper one, whereby the ratio was initialized with a small value (0.4 for T1CE and 0.35 for FLAIR images) and automatically enlarged if leakage occurred. Hence, the upper and lower thresholds of the search range were adapted automatically to the requirements of the actual image without user intervention. Nevertheless, if the segmentation result was not satisfying, the user was allowed to adapt the thresholds. First, the region growing was applied in the T1CE image on a coarse image resolution (3x3x3mm voxel size). The segmented region was then used as starting region for a coarse segmentation in the FLAIR image. Both segmentations were refined on the original image resolution. The segmented hyperintense region in the T1CE image was classified as vital tumor area. A ray search criterion [18] in 2D was used to identify surrounded points which were then classified as necrosis. The remaining segmented hyperintense voxels in the FLAIR image correspond to the perifocal edema.

We applied our segmentation algorithm to 20 clinical routine cases of brain tumors, namely 15 glioblastomas and 5 meningiomas. The images were acquired on a Philips 3T Intera (Best, The Netherlands). The segmentation results were semi-quantitatively validated on two representative slices out of each 3D dataset by two experienced radiologists in consensus. The deviation between segmentation result and visually estimated tumor characteristics was rated on a 5-point scale ranging from "severely under-segmented" to "severely over-segmented". As satisfactory we considered those cases with matching results ("ok") and "slightly under-segmented" or "slightly over-segmented" results.

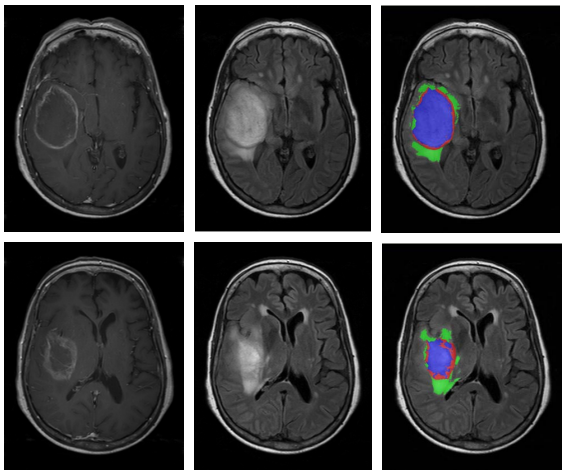

Figure 1: 3D data set of a glioblastoma: T1CE (left), FLAIR (middle), and segmentation result (right, color coded: red = vital tumor, blue = necrosis, green = perifocal edema). The rows show two representative slices out of the 3D data sets.

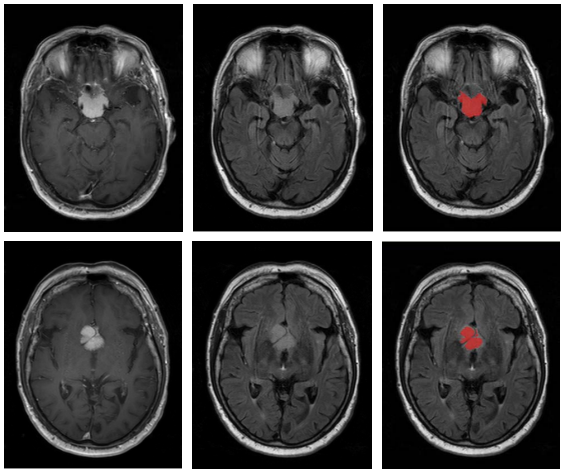

Figure 2: 3D data set of a meningioma. The images are laid out as in Fig. 1.

Results

In 17 out of the 20 clinical test cases we achieved satisfactory results, the validation details can be seen in Table 1. In 9 cases, the tumor rim was very narrow such that the segmented vital tumor area was not closed. Nevertheless, the ray search criterion lead in 89% of these cases to a correct classification of the enclosed necrotic tumor part (see, for instance, Fig. 1). All images revealed strong hyperintense signal around the eyes. If these areas are close to the tumor, region growing algorithms tend to leak out. Our coarse-to-fine approach and the automatic threshold adaptation mostly prevented leakage (see, for instance, Fig. 2). The computation time needed for the whole segmentation and classification process was around ten seconds on a standard personal computer.

Discussion and Conclusions

The proposed algorithm for segmenting and classifying brain tumor tissue yielded satisfactory results in 85% of the clinical test cases. The only required user interaction is a mouse click for providing the starting point. The automatic segmentation result can be altered by adapting the region growing thresholds.

The current version of our segmentation algorithm is only suitable for monofocal tumors. In case of multifocal tumors, the algorithm segments only the part of the tumor which is connected to the user-given starting point. The extension to multifocal tumors will be addressed in our future research.

	severly under-segm.	slightly under-segm.	ok	slightly over-segm.	severly over-segm.
vital tumor	5.0%	32.5%	57.5%	5.0%	0.0%
necrosis	10.0%	0.0%	70.0%	20.0%	0.0%
edema	7.5%	12.5%	50.0%	27.5%	2.5%

Table 1: Validation results for 20 clinical test cases (2 slices out of each data set).

References

[1] Angelini ED et al., Curr. Med. Im. Rev. 3, 262-276, 2007.
[2] Gibbs P et al., Phys. Med. Biol. 41, 2437-2446, 1996.
[3] Konukoglu E et al., Med. Image Anal. 14, 111-125, 2010.
[4] Donahue MJ et al., Magn. Reson. Med. 59, 336-344, 2008.
[5] Müller A et al., Eur. Radiol., Online First, 2010.
[6] Fletcher-Heath LM et al., Artif. Intell. Med. 21, 43-63, 2001.
[7] Liu J et al., Comput. Med. Imaging Graph. 29, 21-34, 2009.
[8] Kaus MR et al., Radiology 218, 586-591, 2001.
[9] Aloui K et al., World Acad. Sci. Eng. Technol. 57, 127-131, 2009.
[10] Ho S et al., Proc. ICPR, 532-535, 2002.
[11] Cobzas D et al., Proc. MMBIA, 2007.
[12] Popuri K et al., Proc. SPIE Med. Imaging, 61441M, 2009.
[13] Moon N et al., Proc. MICCAI, 372-379, 2002.
[14] Capelle A-S et al., Inform. Fusion 5, 203-216, 2004.
[15] Prastawa M et al., Acad. Radiol. 10, 1341-1348, 2003.
[16] Roberts C et al., Proc. ISMRM 18, 2750, 2010.
[17] Opfer R et al., Proc. SPIE Med. Imaging, 2007.
[18] Bülow T et al., Proc. SPIE Med. Imaging, 65140T, 2007.